Crystal Growth & Design, Volume 20, Issue 3, 2020, pp. 1552–1564
DOI: 10.1021/acs.cgd.9b01276

Is chemically reactive membrane crystallisation faciliated by heterogeneous primary nucleation? Comparison with conventional gas-liquid crystallisation for ammonium bicarbonate precipitation in a CO_2-NH_3-H_2O system

S. Bavarella[a], M. Hermassi[a], A. Brookes[b], A. Moore[c], P. Vale[d], G. Di Profio[e], E. Curcio[f], P. Hart[g], M. Pidou[a], E.J. McAdam[a,*]

[a]Cranfield Water Science Institute, Vincent Building, Cranfield University, Bedfordshire, MK43 0AL, UK
[b]Anglian Water Limited, Thorpewood House, Peterborough, UK
[c]Northumbrian Water Limited, Boldon House, Pity Me, Durham, UK
[d]Severn Trent Water Plc, Severn Trent Centre, Coventry, UK
[e]Institute on Membrane Technology, National Research Council of Italy ITM-CNR, Rende, Italy
[f]Department of Environmental and Chemical Engineering, University of Calabria, Rende, Italy
[g]Centre for Energy and Power, Building 52a, Cranfield University, Bedfordshire, Mk43 0AL, UK
*Corresponding author: e.mcadam@cranfield.ac.uk

Abstract

In this study, membrane crystallisation is compared to conventional gas-liquid crystallisation for the precipitation of ammonium bicarbonate, to demonstrate the distinction in kinetic trajectory and illustrate the inherent advantage of phase separation introduced by the membrane to crystallising in gas-liquid systems. Through complete mixing of gas and liquid phases in conventional crystallisation, high particle numbers were confirmed at low levels of supersaturation. This was best described by secondary nucleation effects in analogy to mixed suspension mixed product removal (MSMPR) crystallisation, for which a decline in population density was observed with an increase in crystal size. In contrast, for membrane crystallisation, fewer nuclei were produced at an equivalent level of supersaturation. This supported growth of fewer, larger crystals which is preferred to simplify product recovery and limit occlusions. Whilst continued crystal growth was identified with the membrane, this was accompanied by an increase in nucleation rate which would indicate the segregation of heterogeneous primary nucleation from crystal growth, and was confirmed by experimental derivation of the interfacial energy for ammonium bicarbonate (σ, 6.6 mJ m^{-2}), which is in agreement to that estimated for inorganic salts. The distinction in kinetic trajectory can be ascribed to the unique phase separation provided by the membrane which promotes a counter diffusional chemical reaction to develop, introducing a region of concentration adjacent to the membrane. The membrane also lowers the activation energy required to initiate nucleation in an unseeded solution. In conventional crystallisation, the high nucleation rate was due to the higher probability for collision, and the gas stripping of ammonia (around 40% loss) through direct contact between phases which lowered pH and increased bicarbonate availability for the earlier onset of nucleation. It is this high nucleation rate which has restricted the implementation of gas-liquid crystallisation in direct contact packed columns for carbon capture and storage. Importantly, this study evidences the significance of the membrane to governing crystallisation for gas-liquid chemical reactions through providing controlled phase separation.

Keywords: nucleation; crystal growth; chemical absorption; carbon dioxide; ammonia

Published by ACS. This is the Author Accepted Manuscript issued with: Creative Commons Attribution Non-Commercial License (CC:BY:NC 4.0).
The final published version (version of record) is available online at DOI:10.1021/acs.cgd.9b01276 . Please refer to any applicable publisher terms of use.

1. Introduction

Chemisorption is a mature technology in the oil and gas sector where packed columns are used for carbon dioxide (CO_2) separation in natural gas sweetening, and has seen wide-scale investigation for post-combustion carbon capture and storage (CCS), and biogas enrichment for the production of biomethane[1, 2]. Ammonia (NH_3) has been identified as an excellent substitute for organic amines that are ordinarily used to provide the chemical reaction[3], since it delivers three times the absorption capacity, it is non-corrosive and does not degrade[4,5]. Whilst NH_3 provides the initial chemical reaction with CO_2 leading to the formation of ammonium carbamate:

$$CO_{2(aq)} + NH_3 \leftrightarrow NH_2COOH \quad (1)$$

the overall reaction is best represented by the ionic bond which forms between ionised ammonium (NH_4^+) and bicarbonate (HCO_3^-), to produce ammonium bicarbonate (NH_4HCO_3)[6]:

$$NH_4^+ (l) + HCO_3^- (l) \leftrightarrow NH_4HCO_3(s) \quad (2)$$

Provided concentration of the reactants exceed the solubility product of the salt, crystallisation of NH_4HCO_3 can be achieved. The crystallisation of ammonium bicarbonate has been investigated for inclusion into chemisorption of CO_2 as a method to lower the absorbent mass flow to regeneration. This reduces the process heat demand[7]. However, management of the crystalline solid product within packed columns was difficult, resulting in clogging of the packing[8].

McLeod et al.[9] demonstrated the feasibility of crystallising ammonium bicarbonate at the membrane-liquid interface (shell-side) in a chemically reactive membrane crystallisation reactor (CR-MCr) for biogas upgrading, where the CO_2 partial pressure is ordinarily higher than identified in CCS. In this configuration, a hydrophobic microporous membrane achieves sustained separation of the two phases whilst permitting CO_2 to diffuse through gas filled pores before absorption at the membrane-solution interface[10]. It was proposed that the control of nucleation and crystal growth of ammonium bicarbonate in the segregated liquid phase would simplify the recovery of the crystalline phase. Their study provided the first evidence of membrane contactors for chemically controlled crystallisation in a gas-liquid system. In analogy to membrane crystallisation reactors (MCr) that conventionally use osmotic or thermal gradients to achieve saturation, it is suggested that by providing a more homogeneous distribution of the concentration gradient across the membrane boundary, better control of supersaturation can be mediated to improve control over nucleation[11]. A unique contribution of the chemically reactive MCr is the counter-diffusional driving force of NH_3 and CO_2 that results in supersaturation of the boundary layer which differs markedly from the mixing of two fluids in a packed column, being more analogous to conventional batch crystallisation[12]. For classical membrane crystallisation, the high contact angle of the membrane substrate reduces

the solid-liquid interfacial tension such that the reduction of the energy barrier is sufficient to initiate critical nucleus formation[9,13]. In principle, this combination of a developing concentration gradient at the pore mouth where solid-liquid-gas intersect, and the reduction in free energy promotes the onset of primary heterogeneous nucleation, improving control over the kinetic trajectory and thus control of ammonium bicarbonate crystallisation. Whilst this concept has been proposed, the mechanism has not been explicitly evaluated and the differentiation between the kinetic trajectory provided by the membrane for crystallisation versus conventional crystallisation methods has not been clearly articulated. In this study, we therefore seek to demonstrate the promotion of primary heterogeneous nucleation in chemically reactive membrane crystallisation through using conventional crystallisation technology as a reference to evidence the distinction provided in kinetic trajectories for nucleation and crystal growth by chemically reactive MCr. The following objectives are proposed: (i) Characterise and compare the kinetic trajectories in conventional and membrane assisted crystallisation technologies for ammonium bicarbonate formation; (ii) Seek to differentiate the nucleation mechanism, including primary and secondary effects; (iii) Establish why distinct kinetic trajectories exist for a CO_2-NH_3-H_2O crystallisation solution; and (iv) Quantify product yield and the fate of the nitrogen fraction to evidence any differentiation in the thermodynamic limit for nucleation and growth between the two technologies.

2. Materials and methods

2.1 Fabrication, equipment setup and operation

A Perspex cell was constructed to house a single polypropylene hollow-fibre membrane within a 12mm wide channel (height 5 mm). The hydrophobic microporous membrane provided an interface between the gas phase (CO_2) and the liquid phase (ammonia solution) to permit indirect contact of the two phases. By repelling the aqueous phase, and permitting only the CO_2 gas to diffuse through the pores. The membrane comprised a nominal pore size of 0.2 µm, fractional porosity of 72% and solid-liquid contact angle (θ_{water}) of 117° (Membrana GmbH, Wuppertal, Germany; Table 1). A laminar mass flow controller (0.01-1 L min^{-1}, Roxspur Measurement and Control Ltd., Sheffield, UK) introduced carbon dioxide (99.8%, BOC gases, Ipswich, UK) into the lumen of the hollow-fibre at a flow rate of 1000 ml min^{-1}. The gas flow rate was elevated to ensure negligible resistance to mass transfer provided by the gas phase, and the gas velocity was arbitrarily chosen (gas velocity, 14.7 m s^{-1}). Ammonia solution was recirculated on the shell-side of the membrane between the feed vessel and membrane crystalliser at 200ml min^{-1} (batch operation) with a peristaltic pump (520Du, Watson-Marlow Ltd., Falmouth, UK). The mean residence time in the membrane crystalliser was 3.3s (shell-side priming volume, 11mL; $Q_{shell\text{-}side}$, 200 mL min^{-1}). This generated a localised shear rate of 22 s^{-1} at the membrane wall. The total solution volume (comprising the priming volume,

pipework and downstream vessel) was 200 mL. Consequently, the mean fluid residence time within the downstream vessel was less than 45s. Supplementary mixing was also provided to the vessel by inclusion of a 15mm magnetic stirrer bar, operated at a rotational speed of around 100 rpm to ensure complete mixing" Absorbent temperature was maintained at 5±1°C using a chiller (R1 series, Grant Instruments Ltd., Cambridge, UK). Thermocouples (K-type, Thermosense Ltd., Bucks, UK) were sited upstream and downstream of the cell to record both gas and liquid temperatures.

A conventional gas-liquid batch crystallisation process was developed similar to that proposed[12] for the industrial manufacture of ammonium bicarbonate from carbon dioxide and ammonia. Conventional gas-liquid crystallisers promote the direct mixing of the two phases by bubbling the gas phase (CO_2) through the liquid phase (aqueous ammonia). Carbon dioxide (99.8%, BOC gases, Ipswich, UK) was introduced into a jacketed Duran bottle (500 mL, Soham Scientific, Fordham, UK) through a sintered glass disc diffuser (Hamilton Glass Products Ltd., Surbiton, UK) at 200 mL min^{-1}. TheCO_2 flux was normalised to diffuser surface area ($3x10^{-4}$ m^2). Aqueous ammonia (200 mL) was refrigerated at 5±1°C by cooling with glycerol which recirculated through the glass jacketed feed vessel (R1 Series, Grant Instruments Ltd., Cambridge, UK). Whilst mixing was primarily mediated by gas mixing (Appendix A), the solution was agitated to mix the bulk solution. Due to the restricted solution volume (200mL), the need to retain a gas tight assembly, and limited space for inclusion of an overhead stirrer in the reactor lid, a magnetic stirrer bar was used. The 15mm stirrer bar, was operated at a rotational speed of around 100 rpm (Fisher Scientific, Loughborough, UK). Thermocouples were sited within the gas and liquid phase (K-type, Thermosense Ltd., Bucks, UK) (Figure 1).

2.2 Chemical preparation, sampling and analysis

Aqueous ammonia solutions were prepared by diluting ammonia (35% Fisher Chemicals, Loughborough, UK) into de-ionised water (15.0 MΩ cm^{-1}) to fix concentration between 2.6 and 6.3 mol_{NH3} L^{-1}. Solution pH was adjusted to pH 10 through addition of hydrochloric acid (HCl, 37%, Fisher Scientific, Loughborough, UK) as commonly employed in aqueous ammonia packed column processes[14]. Ammonia concentration was quantified using a proprietary ammonium cell test which pre-acidifes the sample to guarantee quantitation of both nitrogen fractions (NH_3/NH_4^+, VWR International Ltd., Poole, UK). Quantitation was by spectrophotometry (Spectroquant Nova 60, Merck-Millipore, Darnstadt, Germany). Gas flow rate was measured using a bubble flow meter (SKC, Blandford Forum, UK; Restek, Bellefonte, US) and the data used to determine CO_2 flux (J_{CO2}, mol m^{-2} s^{-1}):

$$J_{CO2} = \frac{(Q_{G,in} - Q_{G,out}) \times 273.15 \times 1000}{22.4 \times A_m T_G} \quad (3)$$

where $Q_{G,in}$ and $Q_{G,out}$ are the inlet and outlet gas flow rates ($m^3\ s^{-1}$) respectively, A_m is the membrane surface area (m^2) and T_G is the gas temperature (K)[15]. The development of bicarbonate in solution was determined by UV absorption at 215nm[16] using UV/Vis. Spectrophotometry (Jenway 6715, Cole-Parmer, Stone, UK). Crystal size distribution (CSD) was determined for each level of supersaturation (C/C*) using sacrificial experiments undertaken. For each supersaturation level, sacrificial experiments were undertaken in triplicate, using a new membrane each time. Prior to analysis, the absorbent was filtered through a 0.45 μm filter and weighed (Whatman, Camlab Ltd., Cambridge, UK). The crystals were then immersed in anhydrous alcohol to minimise agglomeration[12] and transferred onto a microscope slide consisting of a 1 mm grid for determination by optical microscopy (Optech Microscope Services Ltd., Thame, UK) using a digital camera (Infinity 3, Lumenera, Ottawa, Canada). Images were analysed with image processing software (Image Pro Plus, Media Cybernetics, Cambridge, UK) to determine crystal number and size. Each image analysed corresponded to around 50 crystals and at least 600 crystals were classified to minimise standard error of the CSD[17].

2.3 Crystallisation kinetics

The probability for preferential heterogeneous nucleation can be described by[18]:

$$\frac{\Delta G_{het}}{\Delta G_{hom}} = 0.25(2+cos\theta)(1-cos\theta)^2\left[1-\varepsilon\frac{(1+cos\theta)^2}{(1-cos\theta)^2}\right]^3 \quad (4)$$

where ΔG_{het} and ΔG_{hom} (J molecule^{-1}) are the Gibbs free energies of heterogeneous and homogeneous nucleation, θ (°) is the contact angle at the liquid-membrane interface, and ε (%) is the fractional porosity of the membrane. The kinetics of nucleation and crystal growth were determined by[19]:

$$G = K_G(c_{fm} - c^*)^g \quad (5)$$

$$B = K_B G^b \quad (6)$$

Where G (m s^{-1}) is the crystal growth rate, B ($N^o\ s^{-1}\ m^{-3}$) is the nucleation rate, K_G ($kg^{-g}\ m^{3g+1}\ s^{-1}$) is the kinetic rate constant for crystal growth, K_B ($No\ m^{-3-b}\ s^{-1+b}$) is the nucleation rate constant, c_{fm} and c* (kg m^{-3}) represent the CO_2(aq) concentrations adjacent to the membrane surface and the equilibrium-saturated concentration at the membrane wall. Exponents *g* and *b* can be experimentally determined through linear regression. If the crystal growth rate is defined as the size variation from L(m) at time t to L+ΔL at t+Δt, then the average crystal growth rate G, over the time interval Δt (s), can be calculated through the linear equation[20]:

$$G(L,t) = \Delta L/\Delta t \quad (7)$$

where G can be experimentally determined at different time intervals and equation 5 converted into its logarithmic form to find K_G and *g* from the intercept and gradient respectively:

$$\log G = \log K_G + g\log (c_{fm} - c^*) \quad (8)$$

In analogy to the growth rate, the nucleation rate can be determined by:

$$B(L,t) = \Delta N/\Delta t \quad (9)$$

where ΔN is the difference in crystal number (N^o m^{-3}) across Δt. The logarithmic form of equation 6 is then used to determine K_B and b from the intercept and gradient respectively:

$$\log B = \log K_B + b\log G \quad (10)$$

According to the classical nucleation theory, the primary nucleation rate (B) is related to supersaturation (S, c_{fm}/c^*) by:

$$B = a\exp\left(\frac{-b}{\ln S^2}\right) \quad (11)$$

The exponential component represents the free energy barrier for critical nucleus formation, the formation of the nucleus, with b (dimensionless) representing the thermodynamic parameter for nucleation, while the kinetic parameter a (N^o s^{-1} m^{-3}) represents the rate at which the barrier is crossed[21]. From linearisation of equation 11, b and a can be estimated from the gradient and intercept respectively of the plot between ln B and $\ln^{-2}S$. Assuming heterogeneous nucleation, then b can be used to determine the interfacial energy (σ, J m^{-2})[22]:

$$b = \frac{\emptyset 16\pi\sigma^3\theta^2}{3(k_BT)^3} \quad (12)$$

where θ is the NH_4HCO_3 molecular volume (8.26×10^{-29} m^3), k_B is the Boltzmann's constant (1.38×10^{-23} J K^{-1}), T is absolute temperature (278.15 K) and ø = $\Delta G_{het}/\Delta G_{hom}$ (~ 0.6) the factor which accounts for the reduction of the Gibbs free energy of the system due to the heterogeneous nucleation on hydrophobic microporous membranes (Equation 4, Table 1). For conventional crystallisation primary and secondary nucleation effects are difficult to discriminate, due to an increased probability the generation of secondary nuclei in the same domain where primary nucleation was initiated[23,24,25]. Consequently, interfacial energy was determined for conventional crystallisation in this study through the method of Nakai which takes into account both primary and secondary nucleation[26,27]:

$$\frac{\beta\sigma}{K_BT} = K \quad (13)$$

where K is a dimensionless parameter dependent on solute (CO_2) concentration and β (m^2) is the geometric factor describing the ammonium bicarbonate crystal[26]:

$$\beta_{cube} = \frac{\varphi_{cube}}{\varphi_{sphere}}\beta_{sphere} \quad (14)$$

where the ratio φ_{cube} / φ_{sphere} introduces a normalisation to shape factor, whilst β_{sphere} can be expressed as a function of NH_4HCO_3 molecular volume:

$$\beta_{sphere} = (4\pi)^{1/3}(3\theta)^{2/3} \quad (15)$$

For reference to the experimentally determined data, the interfacial energy for primary nucleation of ammonium bicarbonate can be determined according to[25]:

$$\gamma = \beta \frac{kT}{V_m^{2/3}} ln\left(\frac{\rho_c}{Mc_{eq}}\right) \quad (16)$$

where γ is interfacial energy (J m^{-2}), V_m is molecular volume (m^3 $molecule^{-1}$), M is the concentration of crystals in suspension (kg m^{-3}) and c_{eq} is the equivalent concentration.

3. Results

3.1 Carbon dioxide absorption chemistry during conventional gas-liquid batch crystallisation

Peak CO_2 flux of around 0.55 $molCO_2$ m^{-2} s^{-1} was recorded at the outset of absorption (Figure 2). A similar flux was sustained in this initial phase up to a supersaturation ratio (C/C*) of 0.5 after which CO_2 absorption reduced rapidly to 0.3 $molCO_2$ m^{-2} s^{-1}. The CO_2 flux then gradually declined over time (Figure 2). Whilst similar initial fluxes were recorded for each ammonia concentration, slightly higher CO_2 fluxes were recorded in the second slower phase of absorption for higher ammonia concentrations. The duration for absorption was also prolonged for higher ammonia concentrations. Solution pH was noted to decline linearly with an increase in CO_2 absorption, as indicated by an increase in the supersaturation ratio (Figure 3). The pH declined more quickly in solutions comprised of lower initial NH_3 concentration. For example, a pH of 7.1 was observed with the 2.6 mol_{NH3} L^{-1} absorbent at C/C* of 1.6, whilst the same pH value was observed at C/C* of 3.2 for the 6.3 mol_{NH3} L^{-1} solution. Interestingly, when the total CO_2 absorbed was normalised with the initial NH_3 concentration, a comparable pH trend from each initial NH_3 concentration was presented (Figure 3b). Absorbance at 215nm was used as a surrogate indicator of bicarbonate development in solution (Figure 4). For each NH_3 concentration, bicarbonate concentration progressively increased to a peak concentration, after which bicarbonate concentration declined. The bicarbonate peak was greatest for the higher ammonia concentrations. The supersaturation ratio at which the peak arose also shifted toward a supersaturation ratio of 1 for higher NH_3 concentrations, which is equivalent to the concentration of absorbed CO_2 required to theoretically crystallise ammonium bicarbonate, assuming all CO_2 was converted to bicarbonate.

3.2 Carbon dioxide absorption chemistry during membrane crystallisation

The CO_2 flow rate delivered to the batch crystalliser was only 200 mL min^{-1}, compared to 1000 mL min^{-1} supplied to the lumen of the hollow fibre membrane. However, a maximum flux of 0.012 $molCO_2$ m^{-2} s^{-1} was recorded for the membrane, in comparison to 0.56 $molCO_2$ m^{-2} s^{-1} for the batch crystalliser (Figure 5). Consequently, to achieve C/C* of 1.8 and 2.6 for the batch crystalliser and MCr required 2.5 and 68 hours respectively. Whilst temporally distinct, the general trend of CO_2 flux was similar between batch crystalliser and membrane. Although both systems comprised of the same initial NH_3 concentration (3.3M), the solution pH of the batch crystalliser was around 0.5 pH unit below the MCr, following the first absorption phase which

is characterised by higher CO_2 fluxes (Figures 2 and 6). Bicarbonate concentration peaked for both crystallisers at a supersaturation ratio of 1. Nitrogen mass balance revealed that of the nitrogen removed from solution, greater than 90% was trapped in the crystalline solid phase in the MCr, compared to only 60% for batch crystallisation, while nitrogen removal recorded a maximum of about 5 and 30% in the MCr and batch crystalliser respectively, indicating an excess of residual reactant in the MCr (Figure 7). From this mass balance, we can assume that of the nitrogen fraction removed during transfer that was not crystallised, instead formed a fugitive emission. This comprises around 7% and 40% of the nitrogen fraction removed from solution during crystallisation, or equivalent to 0.4 and 11.6% of the total available nitrogen for the convention and membrane crystallisers respectively.

3.3 Ammonium bicarbonate crystallisation in batch and membrane operations

A considerably higher nucleation rate was evidenced in the batch crystalliser (Figure 8). To illustrate, the nucleation rate constant K_B and exponent b, were 1.9 x 10^5 No m^{-3-b} s^{-1+b} and 0.38 for MCr and 9.5 x 10^{43} No m^{-3-b} s^{-1+b} and 5.06 for batch crystallisation (Table 2). However, membrane nucleation rate progressively increased following induction, which is comparable to literature on MCr where a thermal gradient was applied to achieve crystallisation[17] (Figure 8). Evaluation of the population density evidenced that following an increase in crystal size, crystal number reduced in the batch crystalliser which is consistent with the literature[12] (Figure 9). In contrast, crystal number increased as crystal size increased in the MCr. The crystal growth rate constant K_G and exponent g determined for MCr were 1.7 x 10^{-14} Kg^{-g} m^{3g+1} s^{-1} and 2.64, and 9.5 x 10^{-8} Kg^{-g} m^{3g+1} s^{-1} and -0.32 for the batch crystalliser, indicating a slower growth rate in MCr which increased with progressive levels of supersaturation, induced through the continued absorption of CO_2 (Figure 10).

4. Discussion

In this study, the decoupling of primary nucleation from secondary nucleation and crystal growth has been demonstrated in a chemically reactive membrane crystallisation reactor. This was confirmed by the increase in population density observed at higher levels of supersaturation for the membrane crystalliser, which occurred despite the continued growth in crystal size (Figure 9). This contradicts the classical behaviour observed in mixed suspension mixed product removal crystallisers (MSMPR) for which secondary nucleation effects dominate subsequently shifting the population balance toward fewer, larger crystals[12]. Such behaviour was observed in the conventional crystalliser (Figure 9), in which primary nucleation can be thought to dominate at the point of induction, but crystal growth is quickly thermodynamically favoured, being undertaken by surface integration of secondary nuclei, the material source being smaller crystals, crystal fragments and supersaturated solution[25]. The

continued production of new nuclei concurrent with crystal growth which was observed in the membrane crystalliser is therefore indicative of the membrane promoting heterogeneous primary nucleation. This is difficult to reconcile from a thermodynamic perspective unless we consider the presence of an alternative thermodynamically favourable substrate to that of existing crystals that can act as a site for new nuclei. The hydrophobic membrane lowers the Gibbs free energy for nucleation (Equation 4), while the counter diffusion chemical gradient raises the local concentration gradient at the membrane wall, the combination of which increase the probability for the continued generation of new nuclei. To support this hypothesis, the interfacial energy was estimated for membrane crystallisation from experimental nucleation data (Table 3)[21,22] as 6.6 mJ m^{-2} which corresponds to the estimated interfacial energy for the primary nucleation of ammonium bicarbonate (Equation 15). Evidence for the formation of nuclei local to the membrane pore structure has been previously presented[9]. To illustrate, at an equivalent supersaturation level (C/C* 1.7), the free energy required for critical nucleus formation is around ΔG^*_{homo} 1.2x10^{-20} J $molecule^{-1}$ for the bulk solution versus only ΔG^*_{hetero} 4.7x10^{-21} J $molecule^{-1}$ through membrane facilitated nucleation (Appendix A). The method of Nakai[26] was used to determine an interfacial energy of 7.7 mJ m^{-2} for the unseeded solution in the batch crystalliser, where the method for estimation was based on combined primary and secondary nucleation effects. The proximity of the model to the estimated interfacial energy for ammonium bicarbonate, supports the influence of secondary nucleation effects in unseeded solution and helps support the distinction between the two crystallisation systems.

Similar CO_2 fluxes were achieved independent of the ammonia concentration (Figure 2), indicating an excess of reactive ammonia[28]. However, at an equivalent NH_3 concentration, a considerably lower CO_2 flux was achieved for the membrane. For chemical absorption within a gas-liquid membrane contactor, three resistances can be related to the overall mass transfer coefficient (K_{ov})[10]:

$$\frac{1}{K_{ov}} = \frac{1}{k_g} + \frac{1}{k_m} + \frac{1}{mk_lE} \quad (17)$$

where is the overall mass transfer coefficient (m s^{-1}), k_g, k_l and k_m are the gas, liquid and membrane mass transfer coefficients (m s^{-1}), and E is the enhancement factor provided by the chemical reaction. Since the gas phase comprised of pure CO_2, we can neglect gas phase resistance, and instead assume that the principle resistance to mass transfer was provided by the sum of the membrane and liquid phases (Heile et al., 2014), the liquid phase accounting for around 90% of the total resistance (Appendix E). Whilst CO_2 transfer in the classical crystalliser was related to the available surface area of the diffuser, the explicit interfacial area for mass transfer is provided by the bubbles formed (Appendix E). Through approximation of the interfacial surface area of the CO_2 bubbles, an analogous CO_2 flux to the membrane

crystallisation reactor is reached, which indicates that raising absolute CO_2 mass transfer may be best accommodated through an increase in membrane surface area[10]. Importantly, the controlled addition of CO_2 at the membrane-solution interface, introduces a counter-diffusional CO_2-NH_3 concentration gradient, to support the creation of a localised supersaturated region[9]. This is evidenced by a comparatively small loss of ammonia from the MCr (Figure 7) which can be ascribed to the laminar hydraulic characteristics of the MCr which minimises the transport of NH_3 to the gas-liquid interface as NH_3 transport is limited to radial diffusion[29], in addition to the effective mediation of the chemical reaction within the boundary layer which confines ammonia through a shift in the ammonia-ammonium equilibrium toward non-volatile ammonium[5]. Nevertheless, low levels of supersaturation were instigated in the chemically reactive MCr which achieved nucleation rates several orders of magnitude below those reported in the literature ranging between 10^5 and 10^8 N^o s^{-1} m^{-3}.[17] Whilst the distinction can be due to hydraulic and geometric characteristics of the crystallisation systems[23], it is proposed that this arises primarily from a considerably lower driving force which can be explained through the two-stage decline in CO_2 flux that was demonstrated during absorption. The initial rapid decline in CO_2 flux is characterised by the fast reaction between CO_2 and NH_3 to form carbamic acid, which reduces solution pH. The rate of pH decline was impingent upon the available CO_2/NH_3 ratio (Figure 3), being governed by the excess of CO_2 (or limited NH_3 concentration)[30]. The reduced pH consequently shifted the ammonia-ammonium equilibrium towards ammonium, which reduces reactivity. Therefore the CO_2 flux reduces due to physical rather than chemical absorption dominating mass transfer in the second stage, the extent that CO_2 flux is sustained was then dependent upon the initial ammonia concentration (Figure 2).[9]

Whilst physical absorption was the dominant mechanism for CO_2 mass transport during induction for both the MCr and batch crystalliser, induction was identified at an earlier supersaturation ratio for the batch crystalliser (Figure 10) which also achieved a considerably higher yield at an equivalent supersaturation ratio (Figure 11). We propose that this occurred due to the direct gas injection used, which induced complete mixing, subsequently lowering metastable zone width (MSZW) providing crystallisation at a lower supersaturation ratio as was evidenced by the production of a comparatively high number of small crystals in this study (Figure 9).[13] When the supersaturation level further increases, combined surface integration and volume diffusion controlled growth take place, coupled with particle agglomeration, which is facilitated by high frequency particle collisions (mainly orthokinetic and inertial collisions), promoted by the shear generated from CO_2 bubbling into the crystallising fluid.[31] It is this production of high crystal number introduced by direct gas mixing of CO_2 and NH_3 which is thought to initiate blocking of packed column technology for CCS.[32] Furthermore, direct gas mixing stripped a higher fraction of free ammonia which reduced the buffering capacity for CO_2, providing a more progressive reduction in pH which increased the availability of HCO_3^-

for crystallisation at an earlier supersaturation ratio. The fugitive loss of ammonia from the conventional crystalliser was demonstrated by the lower nitrogen recovery (Figure 7) and a reduction of pH by around 0.5 unit which occurred following the initial absorption phase. During this initial phase, the equilibrium is shifted toward ammonia (pH >9, Figures 6 and B1). This transition increases the probability for fugitive losses, which limited the subsequent crystal yield in the conventional crystalliser.[5] In contrast, fewer crystals were initially produced from MCr at the outset of crystallisation due to the development of a concentration boundary layer, which constrained dissolution into the bulk fluid. Several authors have also evidenced an increased population density with an increase in supersaturation ratio for MCr using either osmotic or thermal gradients[17,33] which is indicative of the low supersaturation that can be achieved. In this study, the stricter control of nucleation over growth at a lower rate of supersaturation was demonstrated and facilitated the growth of fewer, larger crystals (Figure 9), which are generally thought to be well-shaped with fewer inclusions, and therefore of higher purity[34]. At this low supersaturation rate, crystals did not collect at the membrane surface and were instead primarily encountered downstream. Previous authors have reasoned that the limited membrane crystal deposition was due to the nonspecific and reversible chemical interaction between the membrane and solute.[13] However, at higher free ammonia concentrations, significant membrane crystal deposition has been shown to occur, ostensibly through Ostwald ripening which is an important process in reactive crystallisation.[11,19] Ostwald ripening occurs when particles formed through primary nucleation dissolve to recrystallize onto larger particles. At the ammonia concentration used in this study, a lower rate of primary nucleation is achieved and limited membrane deposition proceeded, as evidenced by the mass balance in which 93% of the ammoniacal nitrogen removed from bulk solution resided within the crystal phase. The continuation of primary nucleation in parallel with crystal growth provides further supportive evidence for Ostwald ripening. As primary nucleation continues to be facilitated by the thermodynamically favourable membrane substrate, primary nuclei are produced that can support the formation of new crystals and the consecutive growth of existing crystals. Analogous behaviour for inorganic salts has also been observed in thermally driven membrane crystallisation.[19] Whilst increasing crystal size by Ostwald ripening leads to a more thermodynamically stable crystal state, it is a slow process[25] and thus may be more conducive to formation within the membrane crystalliser where more controlled conditions for nucleation can be established. Importantly, since the membrane provides a prescribed CO_2 flux, an increase of the membrane-solution interfacial surface area per unit volume, will facilitate a higher yield whilst sustaining control over the nucleation rate.

5. Conclusions

In this study, the kinetics of crystallisation have been confirmed for conventional and membrane crystallisers facilitating a chemical reaction in a gas-liquid CO_2-NH_3-H_2O system. The hydrophobic membrane substrate provides contact between the three phases: membrane, gas and liquid and reduces the activation energy sufficient to induce primary heterogeneous nucleation of ammonium bicarbonate. Through fostering lower rates of supersaturation, fewer nuclei and larger crystals were produced which is beneficial for downstream separation and to control product purity, whilst primary heterogeneous nucleation facilitated by the membrane continued to produce new nuclei which evidences a decoupling of nucleation and growth, which provides improved overall governance of crystallisation in gas-liquid systems. This contradicts behaviour in conventional crystallisation for which primary and secondary effects collectively induce a reduction in particle number with an increase in crystal size; such difficulty in discrimination between mechanisms makes projection of crystal growth difficult to determine. Furthermore, direct mixing in conventional gas-liquid crystallisation induced higher rates of nucleation due to the enhanced probability for collision and the stripping of ammonia which reduced pH to provide a higher bicarbonate concentration at an earlier level of supersaturation. The subsequent loss of free ammonia will reduce the maximum yield of ammonium bicarbonate crystals that is attainable and can be avoided in membrane crystallisation by facilitating indirect contact between the two phases, which limits physical stripping and mediates a shift in equilibrium from ammonia to ammonium to constrain volatility. The yield provided during membrane crystallisation was lower than realised in batch crystallisation which can be explained by the limited specific surface area of the system (<50 $m^2\ m^{-3}$), and the membrane resistance which limited CO_2 flux and solution mixing, and can be improved by an increase in specific surface area and optimisation of hydrodynamics. Importantly, this study evidences the advantage of phase separation facilitated by the membrane for the governance of chemical crystallisation in gas-liquid systems.

Acknowledgements

McAdam and Hermassi would like to thank the European Research Council for financial support (ERC Starting Grant, 714080). Bavarella wishes to thank Anglian Water, Northumbrian Water, Severn Trent Water and the School of Water, Energy and Environment for their financial and technical support, and gratefully acknowledges the resources provided by the Engineering and Physical Sciences Research Council through the STREAM Industrial Doctorate Centre.

Supporting Information

Within the supporting information section, details can be found for the estimation of hydrodynamic shear within the membrane cell and conventional crystalliser (Appendix A), speciation diagrams detailing ammonia and carbon dioxide equilibria at the reference temperature (Appendix B), further description of nucleation rate and the crystal size distributions evolved (Appendix C), and estimation of the interfacial areas for mass transfer within the classical crystalliser to provide an indicative comparative evaluation of carbon dioxide mass transport versus the membrane (Appendix D).

References

[1] Augelletti, R., Conti, M., Annesini, M.C. Pressure swing adsorption for biogas upgrading. A new process configuration for the separation of biomethane and carbon dioxide. J. Clean. Prod. 2017, 140, 1390-1398.

[2] Sahota, S., Shah, G., Ghosh, P., Kapoor, R., Sengupta, S., Singh, P., Vijay, V., Sahay, A., Vijay, V.K., Thakur, I.S. Review of trends in biogas upgradation technologies and future perspectives. Bioresource Technol. Rep. 2018, 1, 79-88.

[3] Bandyopadhyay, A. Amine versus ammonia absorption of CO_2 as a measure of reducing GHG emission: a critical analysis. Clean Technol. Envir. 2011, 13, 269–294.

[4] Makhloufi, C., Lasseuguette, E., Remigy, J.C., Belaissaoui, B., Roizard, D., Favre, E. Ammonia based CO_2 capture process using hollow fiber membrane contactors. J. Membr. Sci. 2014, 455, 236–246.

[5] McLeod, A., Jefferson, B., McAdam, E., 2014. Biogas upgrading by chemical absorption using ammonia rich absorbents derived from wastewater. Water Res. 67, 175-186.

[6] Niu, Z., Guo, Y., Zeng, Q., Lin, W. Experimental studies and rate based process simulations of CO_2 absorption with aqueous ammonia solutions. Ind. Eng. Chem. Res. 2012, 51, 5309-5319.

[7] Gazzani, M., Sutter, D., Mazzotti, M. Improving the efficiency of a chilled ammonia CO_2 capture plant through solid formation: a thermodynamic analysis. Energy Proced. 2014, 63, 1084-1090.

[8] Sutter, D., Gazzani, M., Mazzotti, M. Formation of solids in ammonia-based CO_2 capture processes — Identification of criticalities through thermodynamic analysis of the CO_2–NH_3–H_2O system. Chem. Eng. Sci. 2015, 133, 170-180.

[9] McLeod, A., Buzatu, P., Autin, O., Jefferson, B., McAdam, E. Controlling shell-side crystal nucleation in a gas–liquid membrane contactor for simultaneous ammonium bicarbonate recovery and biogas upgrading. J. Membr. Sci. 2015, 473, 146–156.

[10] Heile, S., Rosenberger, S., Parker, A., Jefferson, B., McAdam, E.J. Establishing the suitability of symmetric ultrathin wall polydimethylsiloxane hollow-fibre membrane contactors for enhanced CO_2 separation during biogas upgrading, J. Membr. Sci. 2014, 452, 37-45.

[11] Bavarella, S., Brookes, A., Moore, A., Vale, P., Di Profio, G., Curcio, E., Hart, P., Pidou, M., McAdam, E.J. Chemically reactive membrane crystallisation reactor for CO2-NH3 absorption and ammonium bicarbonate crystallisation: kinetics of heterogeneous crystal growth, J. membr. Sci. 117682.

[12] Veiga, A.R., Calmanovici, C.E., Giulietti, M. Operational conditions evaluation in ammonium bicarbonate crystallisation. Proceedings of the 14th International Symposium on Industrial Crystallization. 1999, 65, 1−12.

[13] Di Profio, G., Curcio, E., Drioli, E. Supersaturation control and heterogeneous nucleation in membrane crystallizers: facts and perspectives. Ind. Eng. Chem. Res. 2010, 49, 11878–11889.

[14] Yeh, J.T., Resnik, K.P., Rygle, K., Pennline, H.W. Semi-batch absorption and regeneration studies for CO_2 capture by aqueous ammonia. Fuel Process. Technol. 2005, 86, 1533-1546.

[15] Atchariyawut, S., Jiraratananon, R., Wang, R. Separation of CO_2 from CH_4 by using gas–liquid membrane contacting process. J. Membr. Sci. 2007, 304, 163–172.

[16] Wilson, N.S., Morrison, R., Dolan, J.W. Buffers and Baselines. LC-GC Europe. 2001, 1, 1-3.

[17] Ji, X., Curcio, E., Obaidani, S.A., Di Profio, G., Fontananova, E., Drioli, E. Membrane distillation-crystallization of seawater reverse osmosis brines. Sep. Purif. Technol. 2010, 71, 76-82.

[18] Curcio, E., Fontananova, E., Di Profio, G., Drioli, E. Influence of the structural properties of polyvinylideneflouride (PVDF) membranes on the heterogeneous nucleation rate of protein crystals. J. Phys. Chem. B. 2006, 110, 12438-12445.

[19] Chen, G., Lu, Y., Yang, X., Wang, R., Fane, A.G., Quantitative Study on Crystallization-Induced Scaling in High-Concentration Direct-Contact Membrane Distillation. Ind. Eng. Chem. Res. 2014, 53, 15656–15666.

[20] Söhnel, O., Bravi, M., Chianese, A., Mazzarotta, B. Growth kinetics of sodium perborate from batch crystallization. J. Cryst. Growth. 1996, 160, 355-360.

[21] Mersmann, A., Angerhöfer, M., Gutwald, T., Sangl, R., Wang, S. General prediction of median crystal sizes. Sep. Technol. 1992, 2, 85-97.

[22] Gomez-Morales, J., Torrent-Burgues, J., Rodriguez-Clemente, R. Nucleation of calcium carbonate at different initial pH conditions. J. Cryst. Growth. 1996, 169, 331-338.

[23] Curcio, E., Criscuoli, A., Drioli, E., Membrane crystallizers. Ind. Eng. Chem. Res. 2001, 40, 2679–2684.

[24] Agrawal, S.G., Paterson, A.H.J. Secondary Nucleation: Mechanisms and Models. J.Chem. Eng. Commun. 2015, 202, 698-706.

[25] Lewis, A., Seckler, M., Kramer, H., van Rosmalen, G. Industrial Crystallization: Fundamentals and Applications. 1st Edition, Cambridge University Press, Cambridge, UK, 2015.

[26] Nakai, T. Studies of the Estimation of the Interfacial Energy of Embryo in Solid-Liquid Systems. Chem. Soc. Japan. 1969, 42, 2143-2148.

[27] Toyokura, K. New aspects of industrial crystallization. J. Chem. Eng. Jpn. 1995, 28, 361-371.

[28] Esquiroz-Molina, A., Georgaki, S., Stuetz, R., Jefferson, B., McAdam, E.J. Influence of pH on gas phase controlled mass transfer in a membrane contactor for hydrogen sulphide absorption, J. Membr. Sci. 2013, 427, 276-282.

[29] Budzianowski, W.M., Mitigating NH_3 vaporization from an aqueous ammonia process for CO_2 capture, Int. J. Chem. React. Eng. 2011, 9, A58.

[30] Ahn, C.K., Lee, H.W., Lee, M.W., Chang, Y.S., Han, K., Rhee, C.H., Kim, J.Y., Chun, H.D., Park, J.M. Determination of ammonium salt/ion speciation in the CO_2 absorption process using ammonia solution: modelling and experimental approaches. Energy Proced. 2011, 4, 541-547.

[31] Elimelech, M., Gregory, J., Jia, X., Williams, R.A., Particle Deposition and Aggregation: Measurement, Modelling and Simulation. 1st Edition, Elsevier, Amsterdam, 1995.

[32] Yu, H., Qi, G., Wang, S., Morgan, S., Allport, A., Cotterill, A., Do, t., McGregor, J., Wardhaugh, L., Feron, P. Results from trialling aqueous ammonia-based post-combustion capture in a pilot plant at Munmorah Power Station: Gas purity and solids precipitation in the stripper, Int. J. Greenh. Gas. Control 2012, 10, 15-25.

[33] Di Profio, G., Curcio, E., Cassetta, A., Lamba, D., Drioli, E. Membrane crystallization of lysozyme: kinetic aspects. J. Cryst. Growth. 2003, 257, 359-369.

[34] Charcosset, C., Kieffer, R., Mangin, D., Puel, F. Coupling between membrane process and crystallisation operations, Ind .Eng. Chem. Res. 2010, 49, 5489-5495.

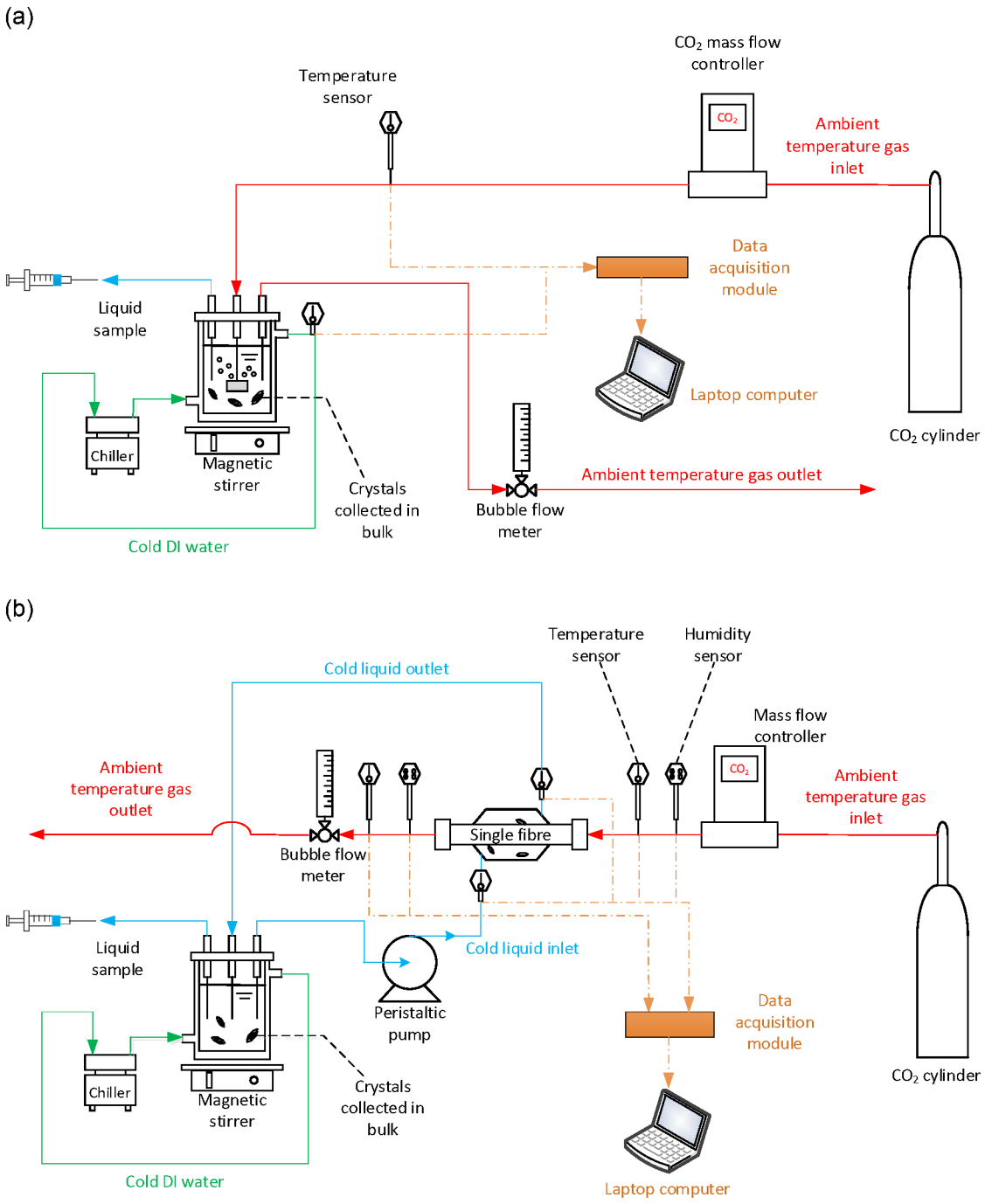

Figure 1. Setup diagrams of batch (a) and membrane (b) chemically assisted crystallisation processes.

(a)

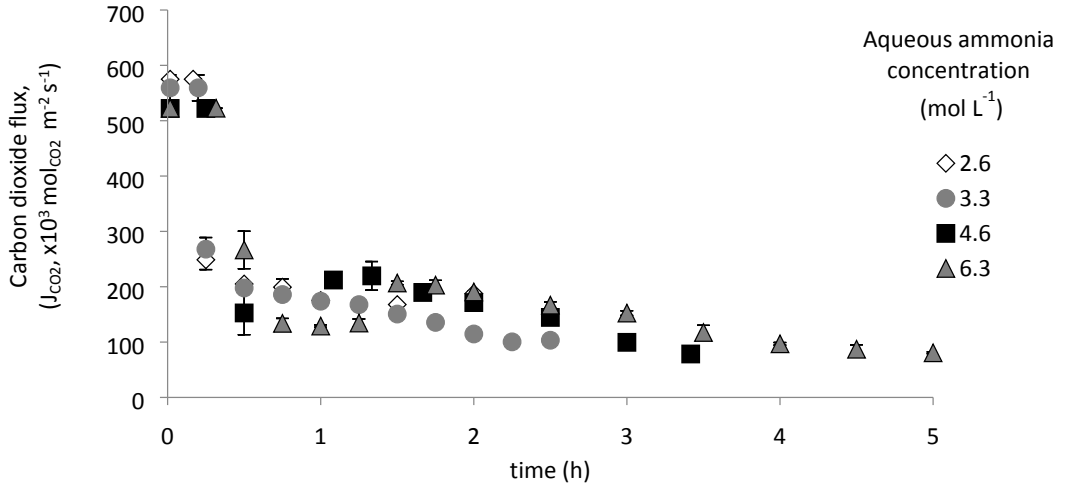

(b)

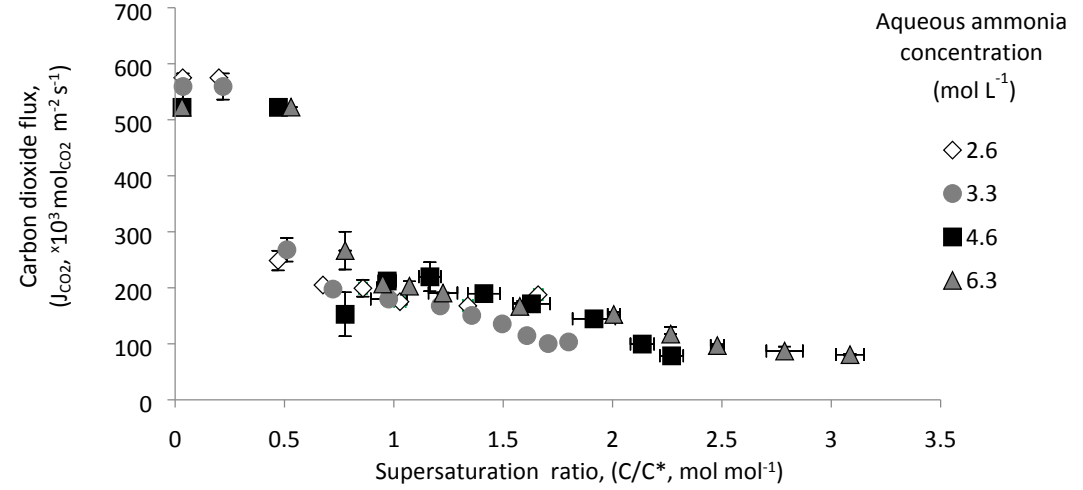

Figure 2. Influence of aqueous ammonia concentration on CO_2 flux decline in batch mode operation. (a) Carbon dioxide flux vs. time; (b) Carbon dioxide flux vs. supersaturation ratio (C/C*, expressed as $CO_{2\ absorbed}$ / $HCO_{3\ saturation}^-$). Error bars indicate standard deviation from sacrificial tests conducted in triplicate.

(a)

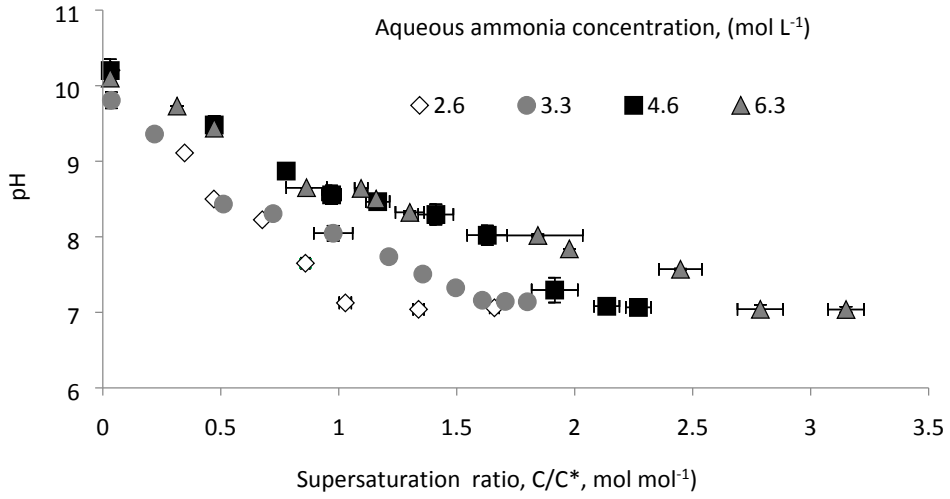

(b)

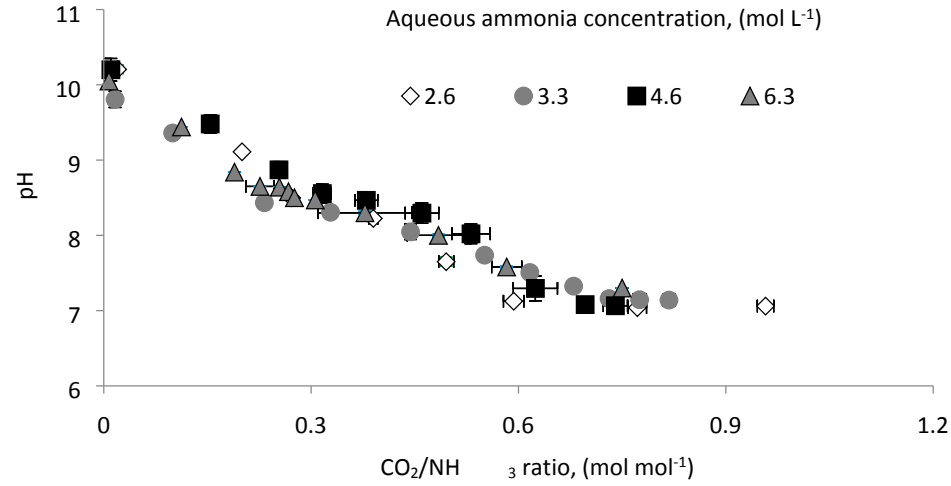

Figure 3. Impact of aqueous ammonia concentration on pH decline as function of supersaturation ratio (C/C* = $CO_{2\ absorbed}$ / $HCO^-_{3\ saturation}$) (a) and CO_2/NH_3 ratio (b) through batch chemically assisted crystallisation. Error bars represent standard deviation of sacrificial experiments undertaken in triplicate.

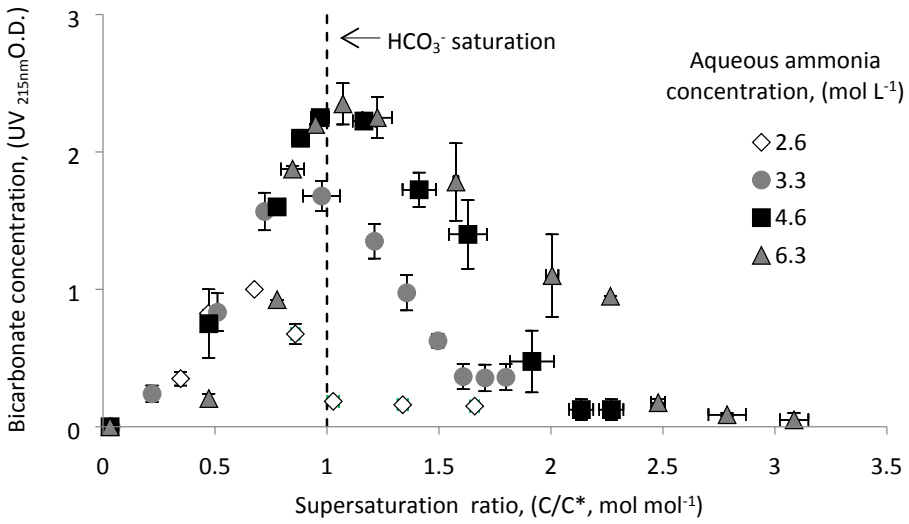

Figure 4. Effect of aqueous ammonia concentration on bicarbonate variation and NH_4HCO_3 crystallisation in batch chemically assisted crystallisation. Carbon dioxide absorbed in solution assumed fully converted into bicarbonate. Error bars indicate standard deviation of sacrificial experiments undertaken in triplicate.

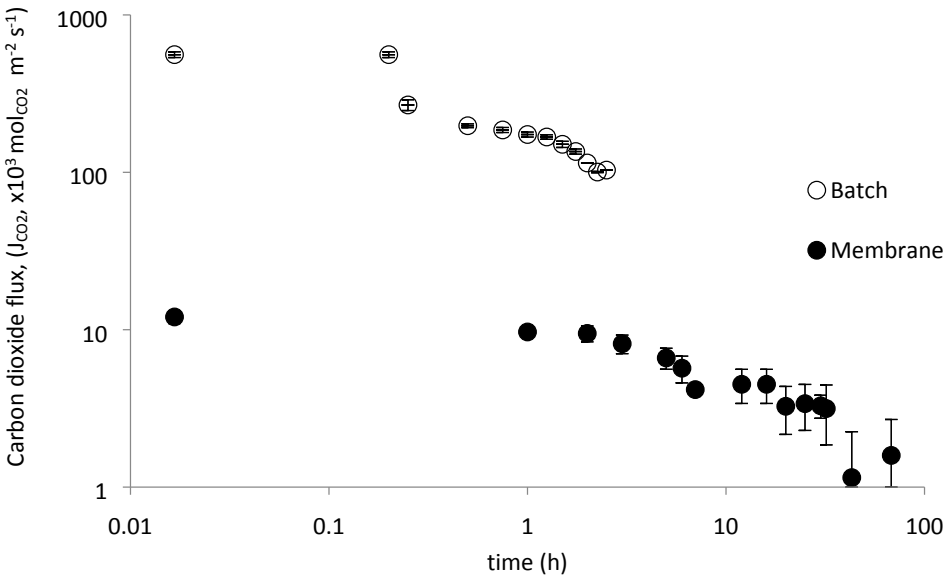

Figure 5. Influence of membrane and batch absorption operations on CO_2 flux decline vs. time. Aqueous ammonia absorbent temperature and concentration of 5°C and 3.3 mol_{NH3} L^{-1} respectively. Error bars indicate standard deviation from sacrificial tests conducted in triplicate.

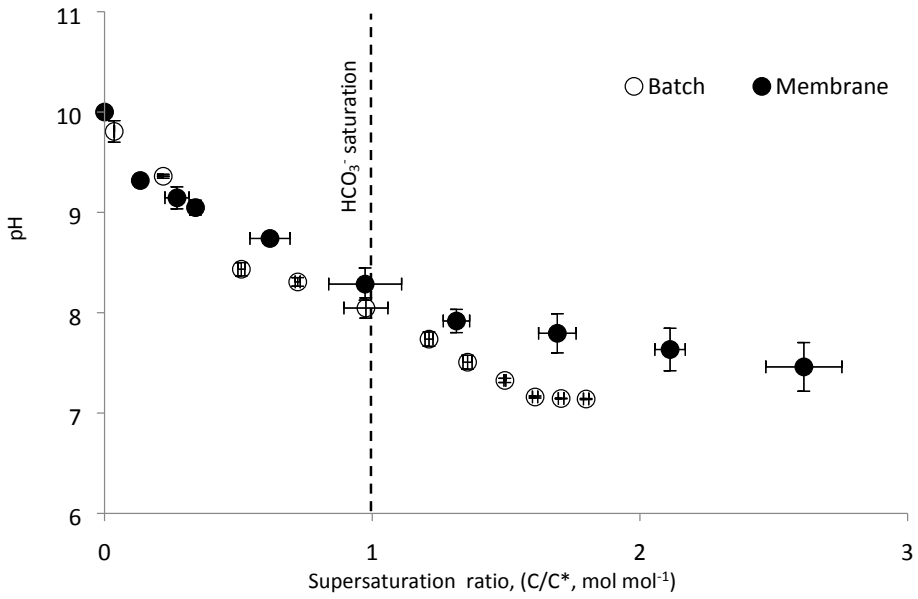

Figure 6. Impact of batch and membrane operation on pH decline as function of supersaturation ratio. Aqueous ammonia absorbent temperature and concentration of 5°C and 3.3 mol_{NH3} L^{-1} respectively. Hydrodynamic conditions: G/L 5, V_L 0.06 m s^{-1} and V_G 14.7 m s^{-1} for membrane crystallisation, while V_L 0.0 m s^{-1} and V_G 0.01 m s^{-1} for batch test (sparger surface area $3x10^{-4}$ m^2). Error bars represent standard deviation of sacrificial experiments undertaken in triplicate.

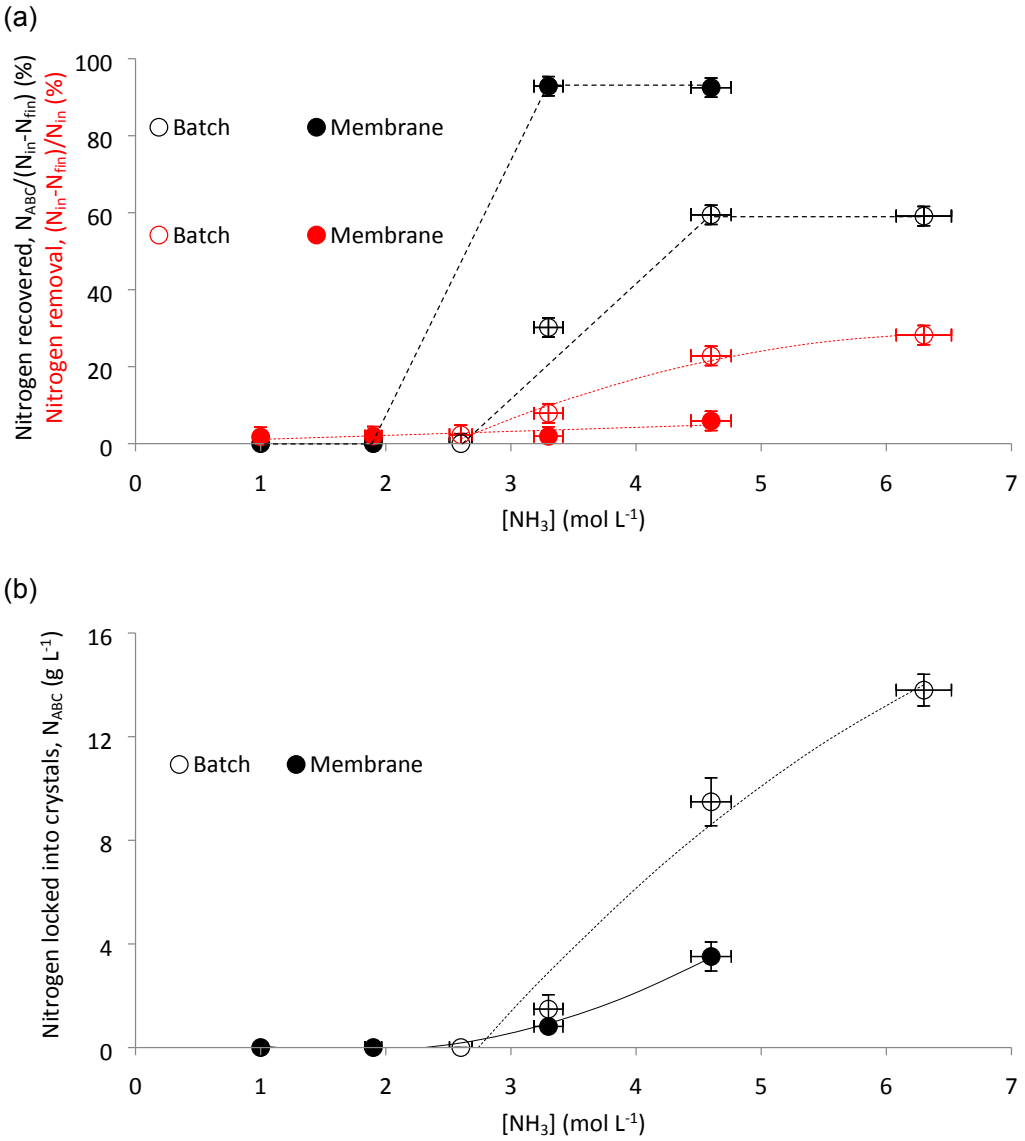

Figure 7. (a) Impact of aqueous ammonia concentration on ammoniacal nitrogen removal, calculated as $(N_{in}-N_{fin})/N_{in}$ (%), where N_{in} and N_{fin} are initial and final ammoniacal nitrogen concentrations (g L^{-1}) (red data points), and recovered, calculated as $N_{ABC}/(N_{in}-N_{fin})$ (%) (black data points), where N_{ABC} is nitrogen concentration locked into the crystals (g L^{-1}, figure b). Liquid volumes: 0.2L and 0.15L for batch and membrane operation, respectively. Error bars indicate standard deviation obtained from sacrificial experiments carried out in triplicate.

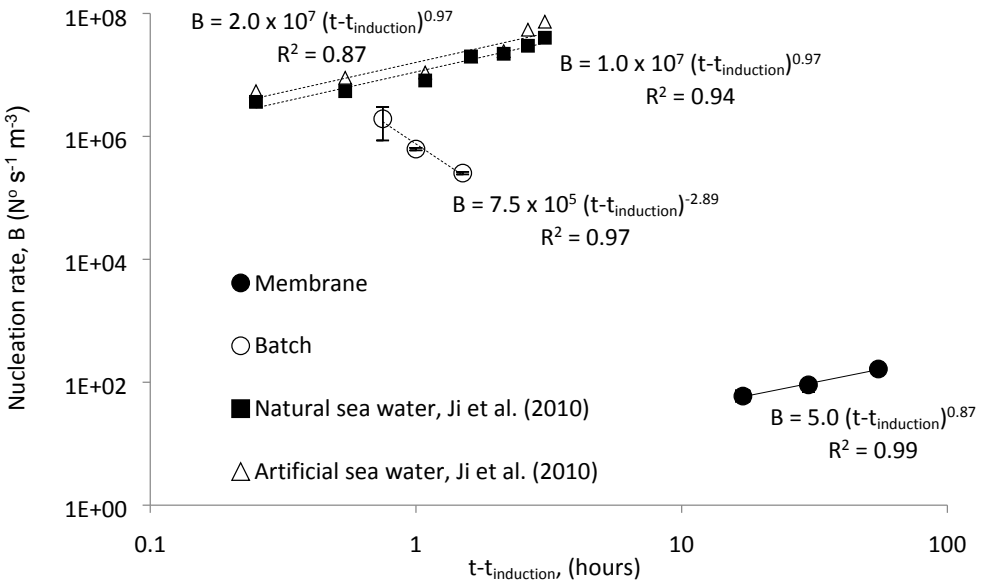

Figure 8. Nucleation rate vs. time (once supersaturation was achieved at induction time) for crystals precipitated in batch and membrane operations. In this study, batch and membrane chemically assisted crystallisation was carried out using aqueous ammonia absorbent temperature and concentration at 5°C and 3.3 mol_{NH3} L^{-1}, respectively. In reference study[17], membrane distillation crystallisation of natural and artificial sea water was undertaken through evaporation-migration-condensation mechanism.

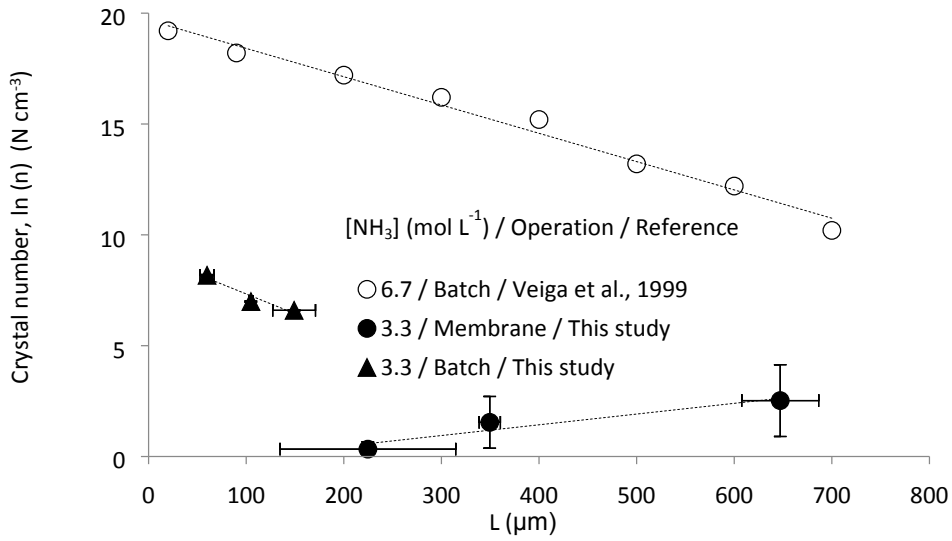

Figure 9. Crystal population density as a function of crystal size undertaken in this study through batch and membrane crystallisation with absorbent concentration of 3.3 mol_{NH3} L^{-1} and temperature of 5°C (black data points), and in reference classical crystalliser[12], using aqueous ammonia concentration of 6.7 mol_{NH3} L^{-1} and temperature of 25°C (white data points). Batch crystallisation operations presented similar population density slopes.

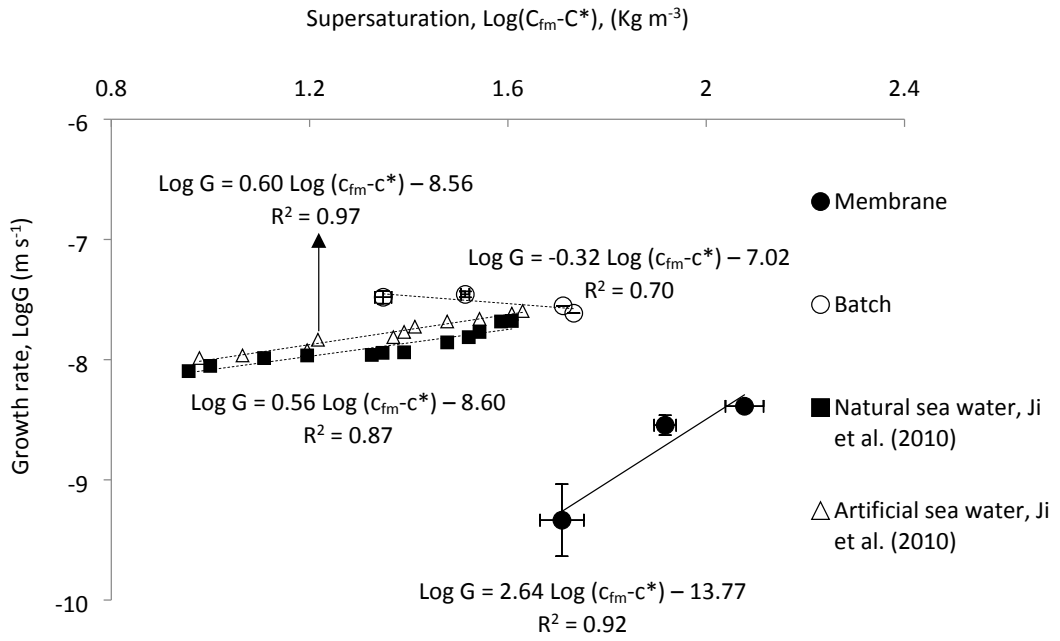

Figure 10. Crystal growth rate vs. supersaturation, where the crystal growth rate constant K_G and exponent for crystal growth g are derived from intercept and slope of experimental data regression. Error bars indicate standard deviation obtained from sacrificial experiments carried out in triplicate in this study.

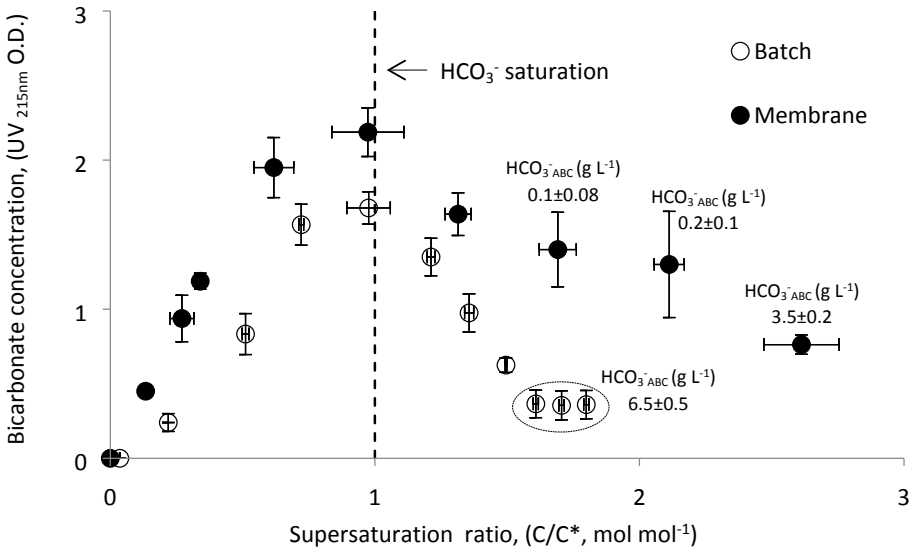

Figure 11. Effect of membrane and batch operation on bicarbonate consumption, where HCO_{3^-ABC} (g L^{-1}) indicates bicarbonate converted into crystal. Liquid volumes are 0.2L and 0.15L for batch and membrane test, respectively. Error bars indicate standard deviation of sacrificial experiments undertaken in triplicate.

Table 1. Dimensions and surface characteristics of the single hollow fibre membrane contactor (HFMC)

		PP
Fibre characteristics		
Membrane material	-	Polypropylene (PP)
Inner diameter	mm	1.2
Outer diameter	mm	1.8
Wall thickness	μm	300
Active length	mm	165
Surface area[b]	m^2	9.33 x 10^{-4}
Porosity	%	72±2[a]
ΔG_{het} / ΔG_{hom}	%	60
Minimum pore size, (d_{min})	μm	0.2[a]
Maximum pore size, (d_{max})	μm	0.36[c]
Contact angle, (θ)	°	117[d]
Lumen cross sectional area	m^2	1.13 x 10^{-6}
Shell side characteristics		
Height	mm	5
Width	mm	12
Shell cross sectional area	m^2	6.0 x 10^{-5}
Priming volume	ml	11.0
Operational characteristics		
Flow regime		Counter-current
Shell-side	M NH_3 (aq)	3.3
Lumen-side		99.8% CO_2
Liquid temperature	°C	5±1
Gas temperature	°C	20±1
Liquid velocity	m s^{-1}	0.06
Gas velocity	m s^{-1}	14.7
Liquid volume in loop	ml	150

[a] Data provided by manufacturer.
[b] Based on fibre outer diameter.
[c] Data statistically determined using log-normal distribution
[d] Bougie and Iliuta (2013)

Table 2. Kinetic expressions for nucleation and growth

Reference	Technology	$G=K_G(c_{fm}-c^*)^g$	$B=K_BG^b$
[17]	[a]MDC	[b]$G=2.8x10^{-9}(c_{fm}-c^*)^{0.60}$	[b]$B=3.7x10^{49}G^{5.52}$
	[a]MDC	[c]$G=2.5x10^{-9}(c_{fm}-c^*)^{0.56}$	[c]$B=8.5x10^{37}G^{3.96}$
This study	Batch	$G=9.5x10^{-8}(c_{fm}-c^*)^{-0.32}$	$B=-9.5x10^{43}G^{5.06}$
	CR-MCr	$G=1.7x10^{-14}(c_{fm}-c^*)^{2.64}$	$B=1.9x10^{5}G^{0.38}$

[a]Membrane distillation-crystallization.
[b]Crystals nucleated from artificial brines.
[c]Crystals nucleated from natural brines.

Table 3. Calculated values of interfacial energies (σ)

Reference	Technology	Interfacial energy, (σ, mJ m^{-2})	Crystal formed
[27]	Fluidized seed bed	10.5	$CuSO_4 \cdot 5H_2O$
	Fluidized seed bed	8.9	K-Alum
	Fluidized seed bed	7.3	$MgSO_4 \cdot 7H_2O$
[17]	[a]MDC	[b]9.6; [c]10.2	NaCl
This study	CR-MCr	6.6	NH_4HCO_3
	Batch	7.7	NH_4HCO_3

[a]Membrane distillation-crystallization.
[b]Crystals nucleated from artificial brines.
[c]Crystals nucleated from natural brines.

For Table of Contents List only

Is chemically reactive membrane crystallisation faciliated by heterogeneous primary nucleation? Comparison with conventional gas-liquid crystallisation for ammonium bicarbonate precipitation in a CO_2-NH_3-H_2O system

S. Bavarella[a], M. Hermassi[a], A. Brookes[b], A. Moore[c], P. Vale[d], G. Di Profio[e], E. Curcio[f], P. Hart[g], M. Pidou[a], E.J. McAdam[a,*]

[a]Cranfield Water Science Institute, Vincent Building, Cranfield University, Bedfordshire, MK43 0AL, UK
[b]Anglian Water Limited, Thorpewood House, Peterborough, UK
[c]Northumbrian Water Limited, Boldon House, Pity Me, Durham, UK
[d]Severn Trent Water Plc, Severn Trent Centre, Coventry, UK
[e]Institute on Membrane Technology, National Research Council of Italy ITM-CNR, Rende, Italy
[f]Department of Environmental and Chemical Engineering, University of Calabria, Rende, Italy
[g]Centre for Energy and Power, Building 52a, Cranfield University, Bedfordshire, Mk43 0AL, UK
*Corresponding author: e.mcadam@cranfield.ac.uk

Table of contents entry

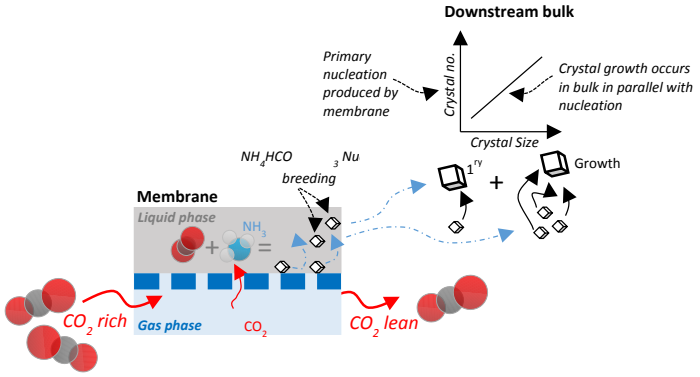

The trajectory for nucleation kinetics in membrane crystallisers is different to that for classical crystallisation, showing an increase in nucleation rate in parallel with an increase in crystal growth. This is accounted for by the membrane which provides greater control for nucleation, ostensibly supporting Ostwald ripening effects.

https://dspace.org/

Is chemically reactive membrane crystallisation faciliated by heterogeneous primary nucleation? Comparison with conventional gas-liquid crystallisation for ammonium bicarbonate precipitation in a CO2-NH3-H2O system

Bavarella, Salvatore; Hermassi, Mehrez; Brookes, Adam; Moore, Andrew; Vale, Peter C. J. ...

2020-01-27
American Chemical Society
https://doi.org/10.1021/acs.cgd.9b01276
Bavarella S, Hermassi M, Brookes A, et al., (2020) Is chemically reactive membrane crystallisation faciliated by heterogeneous primary nucleation? Comparison with conventional gas-liquid crystallisation for ammonium bicarbonate precipitation in a CO2-NH3-H2O system. Crystal Growth and Design, Volume 20, Issue 3, March 2020, pp. 1552-1564

Downloaded from a DSpace repository. https://dspace.org/